



Gravity waves and momentum fluxes in the mesosphere and lower thermosphere using 430 MHz dual-beam measurements at Arecibo:

1. Measurements, methods, and gravity waves

Diego Janches,¹ David C. Fritts,¹ Dennis M. Riggin,¹ Michael P. Sulzer,² and Sixto Gonzalez²

Received 10 November 2005; revised 23 May 2006; accepted 30 June 2006; published 28 September 2006.

[1] We report here and in a companion paper by Fritts et al. (2006a) on a new use of the UHF radar at the Arecibo Observatory in Puerto Rico. We have employed the 430 MHz radar for incoherent scatter measurements of radial wind spectra at altitudes from ~ 71 to 95 km using the Gregorian and line-feed antennas to define beam angles inclined 15° to the east and west of zenith. We find that the two beams define radial velocities with sufficient accuracy to characterize both the gravity waves and the momentum fluxes due to these waves over the majority of the observed altitude range during daylight hours. The characteristics of the gravity waves inferred from these measurements include (1) vertical scales ranging from ~ 2 to 20 km, (2) downward phase progression of the dominant gravity waves up to $\sim 5 \text{ ms}^{-1}$, and (3) vertical wave number spectra having slopes near a value (-3) expected for saturated gravity waves. Gravity wave frequency spectra and momentum fluxes are addressed in the companion paper.

Citation: Janches, D., D. C. Fritts, D. M. Riggin, M. P. Sulzer, and S. Gonzalez (2006), Gravity waves and momentum fluxes in the mesosphere and lower thermosphere using 430 MHz dual-beam measurements at Arecibo: 1. Measurements, methods, and gravity waves, *J. Geophys. Res.*, *111*, D18107, doi:10.1029/2005JD006882.

1. Introduction

[2] Incoherent scatter (IS) radars have been employed for three decades to study the dynamics and electrodynamics of the mesosphere, thermosphere, and ionosphere (MTI). Doppler measurements of neutral winds have provided information on mean winds, large-scale tidal structures, and smaller-scale gravity waves (GWs) in the mesosphere and lower thermosphere (MLT) [Woodman and Guillen, 1974; Mathews, 1976; Ganguly, 1980; Fukuyama, 1981; Fukao et al., 1985; Hocke and Schlegel, 1996; Oliver et al., 1997; Zhou et al., 1997; Larsen, 2000; Zhou, 2000]. Backscatter power and electron density measurements have yielded signatures of GWs having larger spatial scales, penetrating to much higher altitudes, and triggering neutral-plasma interactions [Mathews et al., 1997; Djuth et al., 1997, 2004; Nicolls and Kelley, 2005]. Only recently, however, have measurement techniques at Arecibo Observatory (AO) enabled the collection of IS data having high spatial and temporal resolution and high neutral wind accuracy [Zhou, 2000]. Together with the recent upgrade of the 430 MHz radar to a dual-beam configuration, these capabilities now allow for direct measurements at AO of the

vertical flux of horizontal momentum by atmospheric GWs at MLT altitudes. Our purposes in this and the companion paper by Fritts et al. [2006a] are to employ these new measurement capabilities for dual-beam studies of GW structure, variability, and momentum fluxes in the MLT at AO. If such measurements prove to be sufficiently accurate, and if there is a potential for similar full diurnal measurements in the future, even at much coarser spatial and temporal resolution, then such AO measurements may play a key role in defining the correlations between GW momentum fluxes and diurnal tidal amplitudes and phases that will surely play a major role in improved parameterizations of such interactions and MLT effects because of the location of AO (18.3°N) near the latitude of the maximum diurnal tidal response in the zonal wind field.

[3] While gravity waves (GWs) have significant and systematic effects at lower altitudes [Hitchman et al., 1989; Kim et al., 2003], their major influences are exerted at greater altitudes where GW energy densities and momentum fluxes, relative to mean densities, are much larger. GWs are now known to provide the major forcing of the MLT through the vertical transport of horizontal momentum. These GWs are excited primarily by orography, convection, wind shears, and jet streams at lower altitudes [Fritts and Nastrom, 1992], and they propagate obliquely upward with group and phase velocities that depend on intrinsic properties that vary in altitude. Because motions within a GW field are along their phase lines, their horizontal and vertical velocities are either in phase or antiphase, leading to a momentum flux that is significant for GWs having large

¹Colorado Research Associates, NorthWest Research Associates, Boulder, Colorado, USA.

²Arecibo Observatory, National Astronomy and Ionosphere Center, Arecibo, Puerto Rico.

amplitudes and intrinsic frequencies (see the review by *Fritts and Alexander* [2003]).

[4] Momentum flux divergence arising from GW dissipation processes is the major cause of the departure of the MLT from radiative equilibrium conditions. The zonal decelerations resulting from momentum flux divergence reverses the vertical shear of the zonal wind and “closes” the mesospheric jets above ~ 50 to 90 km at middle and high latitudes in both summer and winter hemispheres [*Holton*, 1982; *Garcia and Solomon*, 1985]. This “GW drag” is balanced by the Coriolis torque on an induced mean meridional circulation from the summer to the winter hemisphere near the mesopause that also causes upwelling and cooling in summer and subsidence and warming in winter, thus driving the MLT far (~ 50 K) from radiative equilibrium conditions [*McIntyre*, 1989].

[5] Mean zonal momentum fluxes (per unit mass) are typically ~ 5 to $15 \text{ m}^2 \text{ s}^{-2}$ and mean decelerations may reach ~ 50 to $100 \text{ ms}^{-1} \text{ day}^{-1}$ in the MLT at middle and high latitudes, though peak values accompanying small-scale, large-amplitude GWs may be much larger (*Fritts and Alexander* [2003] for a review of these dynamics). Indeed, the variability of GW forcing likely has many additional influences, only some of which we have likely anticipated and/or observed to date. Surely a major influence is GW filtering by, and modulation of, tidal and planetary wave (PW) motions, where, despite efforts to date, major uncertainties remain [*Walterscheid*, 1981; *Fritts and Vincent*, 1987; *Forbes et al.*, 1991; *Wang and Fritts*, 1991; *Lu and Fritts*, 1993; *McLandress and Ward*, 1994; *Nakamura et al.*, 1997; *Murphy and Vincent*, 1998; *Mayr et al.*, 1998; *Meyer*, 1999a, 1999b; *McLandress*, 2002]. Large-amplitude GWs also lead to strong local instabilities and strong turbulence and mixing [*Fritts et al.*, 1993, 1994, 1996, 1998, 2002, 2003, 2006b; *Swenson and Mende*, 1994; *Andreassen et al.*, 1994, 1998; *Hecht et al.*, 1997, 2000, 2005; *Yamada et al.*, 2001; *Williams et al.*, 2002; *Hecht*, 2004; *Li et al.*, 2005a, 2005b, 2005c] as well as excitation of additional GW motions [*Vadas and Fritts*, 2001, 2002; *Vadas et al.*, 2003]. Despite these advances, there remain major unknowns concerning GW forcing and effects in the MLT and extending to higher altitudes (see the review by *Fritts and Alexander* [2003] for an extensive discussion). Examples include (1) the influences of specific lower atmosphere GW sources and their variability in the MLT and above; (2) uncertainties over the magnitude (and even the sign!) of GW influences on tidal (and PW) amplitudes; (3) the influences of GW interaction and instability dynamics on the evolution of the GW spectrum with altitude; (4) the role of GW instability in mixing and transport of momentum, heat, and constituents; (5) the penetration and solar cycle modulation of GW forcing at thermospheric altitudes; and (6) the role of GWs in plasma dynamics and instabilities in the ionosphere.

[6] The above discussion provides strong motivations for an accurate determination of GW characteristics, and especially momentum fluxes, over extended altitudes in the MLT wherever such measurements can be performed. Here and in the companion paper by *Fritts et al.* [2006a], we will employ the new dual-beam AO 430 MHz measurement capabilities to define the GW spatial and temporal scales, spectra, momentum fluxes, and the variability of these quantities during two initial 2-day measurement intervals

that we employed to test the potential for these new measurements. This paper includes a discussion of the data collection and analysis methods (section 2) and the observed GW structures and their vertical wave number spectra (section 3). A summary and discussion of the relevance of these observations and our conclusions are provided in sections 4 and 5. Discussion of GW frequency spectra, momentum fluxes, their correlations with the large-scale wind field, and their spatial and temporal variability is provided in the companion paper.

2. Data Collection and Analysis

2.1. Data Collection

[7] We employed the AO 430 MHz transmitter operating at a peak power of 2 MW and using a 13-baud Barker code (1 1 1 1 1 -1 -1 1 1 -1 1 -1 1), a baud length of $4 \mu\text{s}$ (a range resolution of 600 m), and an IPP of 1.04 ms to sample the velocity field between 57.6 and 108 km range using the incoherent scatter technique. The power was split between the Gregorian and the line feeds to create two beams inclined 15° east and west of vertical. The first measurement interval of ~ 7.4 hours during daytime on 11 September 2005 used the Gregorian viewing east and the line feed viewing west. The second measurement interval of ~ 6.7 hours during daytime on 12 September 2005 reversed the two feeds. Received signals were oversampled at 150 m resolution, Doppler spectra were obtained using 256 samples, spectra were averaged for 2.27 min to improve signal-to-noise (S/N), and radial velocities were obtained by fitting a Lorentzian function to the spectra following dc and background removal. Oversampling improved the duty cycle, S/N, and velocity uncertainties, but did not improve altitude resolution.

2.2. Data Analysis

[8] Examples of fitted spectra at several different altitudes are shown in Figure 1. The difficulty in getting good velocity estimates at altitudes below 71 km is due to the signal strength. The spectra here are very narrow because of the increasing collision frequency, decreasing temperature, etc., so the pulse-to-pulse technique we employed is valid, but without sufficient signal (electron densities), the noise level is very high and the S/N is not adequate (see Figure 1a). Negative ions also likely contributed to greater spectral broadening at the lower altitudes than would have occurred in their absence. At higher altitudes (>95 km), spectra widths increase with altitude because of the decreasing collision frequency, increasing temperature, etc., the spectral width is greater than the resolved spectrum, and the pulse-to-pulse technique fails.

[9] Lorentzian fits to spectra in the ~ 71 to 95 km altitude range were performed after subtraction of the estimated noise, computed at the edge of each spectrum, and yielded very good radial velocity estimates over this range. Radial velocities were relatively low, and aliasing was not a problem for the altitude interval analyzed. By fitting a folded Lorentzian function, we could potentially extend the upper altitude interval over which usable velocity estimates can be obtained, but that is left for a future paper.

[10] The radial wind estimates resulting from the procedures described above are shown at 600-m intervals for both

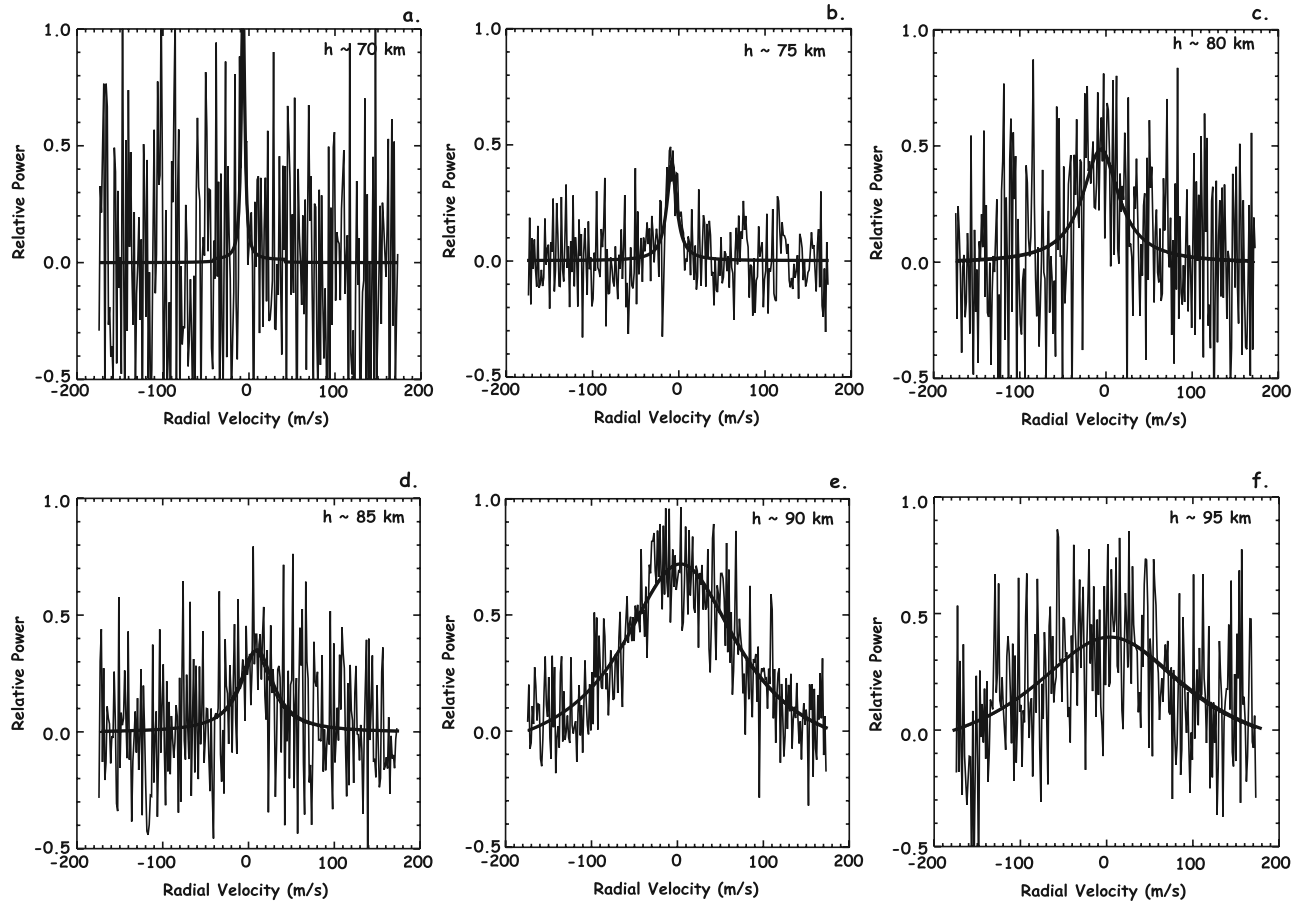


Figure 1. Representative Doppler spectra at (a) 70, (b) 75, (c) 80, (d) 85, (e) 90, and (f) 95 km obtained with the methods described in section 2. S/N decreases sharply at lower altitudes, while the spectral width broadens considerably at the higher altitudes.

east and west beams for each day in Figures 2 and 3. Outliers were removed from the raw time series because of the need to reduce variance errors as much as possible for the momentum flux estimates described in the companion paper by *Fritts et al.* [2006a]. The outlier rejection scheme removed velocity estimates that differed from neighboring values at the same altitude by more than 25 ms^{-1} or from estimates at adjacent (independent) altitudes (at a 600-m spacing) by more than 5 ms^{-1} . The resulting time series have each had a linear trend removed, successive time series are displaced by 20 ms^{-1} , and the velocity scale is shown on the left axis in each panel. Radial velocity uncertainties were typically $\sim 1 \text{ ms}^{-1}$ on the basis of the confidence in the individual Lorentzian spectral fits (see the estimated radial velocity error variances in Figures 4b and 4d), and the larger uncertainties occurred at the highest altitudes where the spectra became very broad (see Figure 1). Radial velocity variances computed from the data displayed in Figures 2 and 3, in contrast, were ~ 10 to 40 times larger (see Figures 4a and 4c), yielding high confidence in the radial velocities and in the variances, spectra, and fluxes derived from them below and in the companion paper by *Fritts et al.* [2006a]. The close agreement between the two beams in estimates of radial velocity variances and uncertainties (Figure 4), and the resulting lack of bias in momentum flux estimates when no significant GW activity was present [see *Fritts et al.*, 2006a],

suggest that the balanced gains and narrow beam widths obtained with the Gregorian and line feeds at 430 MHz imposed no measurement biases on our data.

[11] Because of the baud length employed in the Barker code, velocities at successive altitudes in Figures 2 and 3 are independent estimates. Yet they exhibit very high coherence between adjacent altitudes, suggesting high confidence in the velocities obtained with our spectral fitting and noise suppression methods described above. The lower-frequency motions (periods of ~ 1 to 7 hours) also exhibit considerable coherence between beams (though they are oppositely correlated) because these motions are largely horizontal, have large horizontal scales, and thus project oppositely into the two beam directions. In contrast, higher-frequency motions (periods of ~ 5 to 30 min) often exhibit similar periodicities at the same altitudes and times, but they do not exhibit correlated phase structures between the two beams because these motions occur on smaller horizontal scales (often comparable to or less than the beam spacing at MLT altitudes) and include significant vertical velocity contributions to the measured radial velocities, which are not expected to exhibit coherence at these spatial scales. Radial velocities achieve magnitudes of ~ 5 to 15 ms^{-1} in the east and west beams on both days, but are typically ~ 2 times larger at times of, and in the direction of, significant momentum fluxes [see *Fritts et al.*, 2006a].

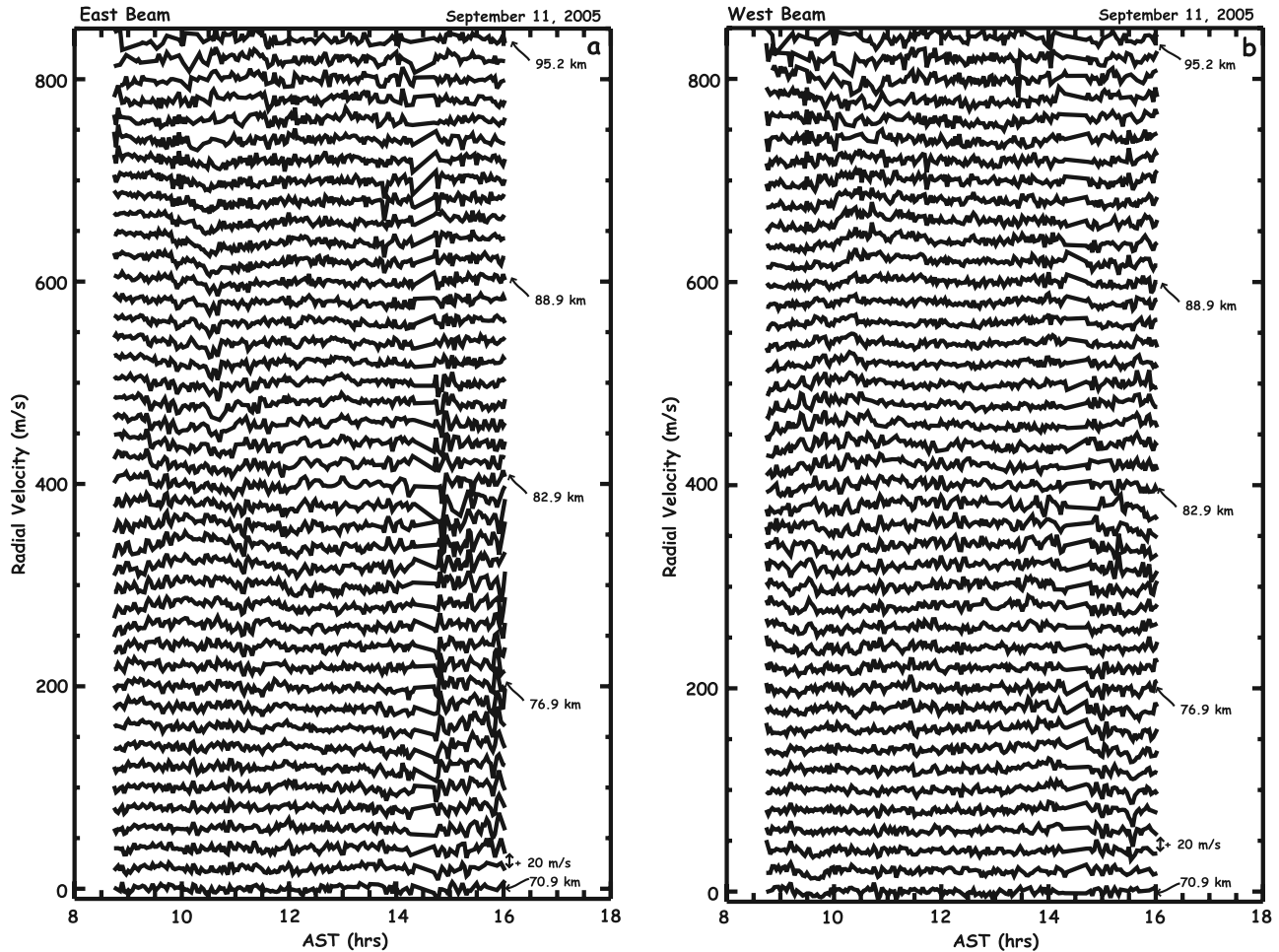


Figure 2. Radial wind estimates in the (left) east and (right) west beams at 600-m intervals from 71 to 95 km obtained on 11 September 2005. The amplitude scale is shown on the left axis, measurements at successive 600-m altitudes are displaced by 20 ms^{-1} , and altitudes are identified at $\sim 6\text{-km}$ intervals.

[12] These data are impressive in both their continuity and apparent accuracy. In contrast, other radars (typically MF and VHF) do not achieve the extended, and continuous, altitude coverage (~ 71 to 95 km), the spatial and temporal resolution (600 m and 2.27 min), or the velocity accuracy. Rayleigh and resonance lidars do cover extended altitudes, typically ~ 30 to 80 km for Rayleigh and ~ 80 to 105 km for Na resonance, and yield high spatial and temporal resolution, but these data must be averaged significantly to achieve sufficient accuracy, and their performance is significantly degraded during daytime where narrowband filters are required. Finally, in situ probes provide either very high spatial resolution, but only a single profile (typically ion, electron, or neutral density measurements), or coarser spatial and temporal resolution (falling spheres).

3. GW Characteristics and Vertical Wave Number Spectra

[13] To further quantify the above statements, we show in Figure 5 eight $\sim 55\text{-min}$ averages of the inferred eastward winds computed separately from each beam for 11 September (~ 22.5 velocity estimates in each average) and eight $\sim 50\text{-min}$ averages for 12 September (~ 20 velocity esti-

mates in each average). There are differences between the eastward winds inferred with the east and west beams, but these display no systematic differences below ~ 90 km that cannot be attributed to horizontal phase differences between the beams and/or the influences of small vertical velocities even in $\sim 50\text{-min}$ averages. At higher altitudes, there are systematic differences, but these have the same tendency (an apparent mean vertical motion that increases to larger negative values with altitude), because the departures between the two beams are the same sign even though the two antennas were switched in their pointing directions on the two days. Uncertainties in the horizontal wind estimates are typically ~ 2 to 4 ms^{-1} (vertical velocity errors are averaged out, but horizontal errors are increased by 4 times) and are smaller than the differences discussed above.

[14] The zonal wind profiles shown in Figure 5 exhibit vertical wavelengths ranging from ~ 2 to 20 km, generally downward phase progression as large as $\sim 0.5 \text{ ms}^{-1}$, GW amplitudes and wavelengths apparently increasing with altitude, and wind shears that approach $\sim 40 \text{ ms}^{-1} \text{ km}^{-1}$ at various locations and times (with isolated values almost twice as large). All these wind features are typical of lower-frequency motions observed at similar altitudes at other locations. In particular, the vertical wavelength and phase

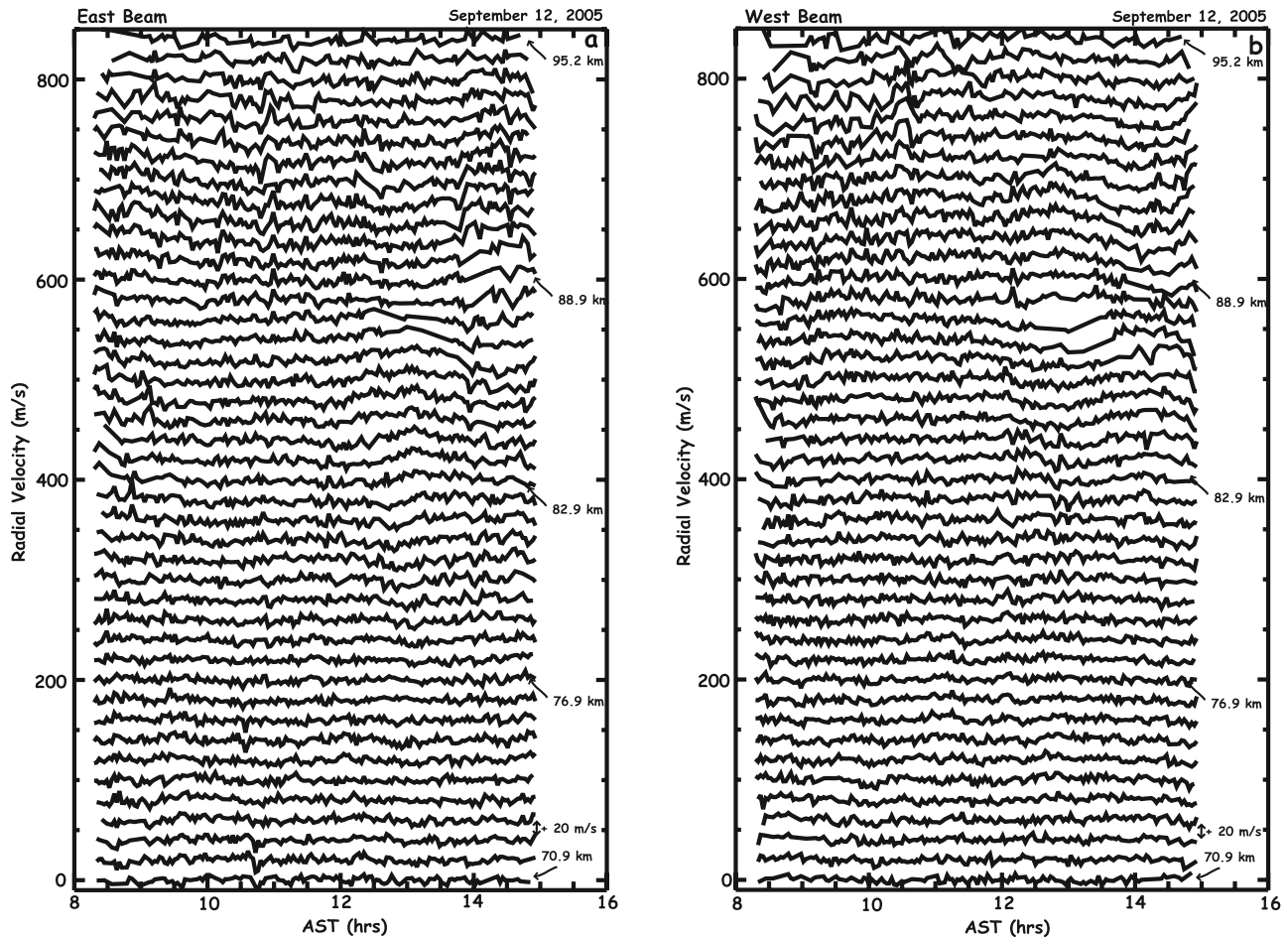


Figure 3. As in Figure 2 but for the radial velocities measured on 12 September 2005.

descent of the largest-scale motion (~ 20 km) seen on 12 September are not inconsistent with the diurnal tidal structure at the latitude of AO, so a contribution to the motion field by the diurnal tide is possible, indeed likely. The ~ 7 -hour mean winds shown in Figures 5b and 5d surely include signatures of the zonal mean wind and the diurnal tidal structures, expected to have significant amplitudes at these altitudes and this latitude [Hagan and Forbes, 2002]. One cannot say more about tidal contributions, however, without considerably more data, either full diurnal measurements or multiple days exhibiting consistent phase behavior. The large wind shears seen in Figure 5 are also of interest, as they are an indication of the potential for local GW instability processes and GW-mean flow interactions. This is because a GW wind shear, du'/dz , comparable to or larger than the local buoyancy frequency, is evidence of overturning within the GW field [Fritts and Alexander, 2003]. We also know that this threshold is well above GW amplitudes that readily trigger other types of instabilities [Klostermeyer, 1991; Lombard and Riley, 1996; Sommor and Klaassen, 1997; Fritts et al., 2003, 2006b]. However, the GW components to the zonal mean winds are likely averaged to a greater degree than the zonal mean and tidal motions in these data.

[15] The systematic differences in the zonal winds inferred from the east and west beams above ~ 90 km in Figure 5 suggest biases in the mean vertical motions

comparable to those seen with other radars. To explore this further, we employ the \sim hourly averaged data to estimate the inferred vertical motions in Figure 6. The apparent vertical motions increase from ~ 1 to 3 ms^{-1} oscillatory motions below 90 km to $\sim 5 \text{ ms}^{-1}$ systematic downward motions at ~ 95 km. These apparent downward motions at the highest altitudes cannot be accurate estimates of the mean vertical motion, as there is not an indication of the very large adiabatic heating that these would imply. However, there have also been a number of previous radar inferences of downward mean vertical motions of $\sim 1 \text{ ms}^{-1}$ or larger at mesopause altitudes, and of similar, but smaller, tendencies at lower altitudes [Balsley and Riddle, 1984; Nastrom et al., 1985; Green et al., 1988; Fritts and Yuan, 1989; Meek and Manson, 1989; Fritts et al., 1990; Rüster and Reid, 1990; Wang and Fritts, 1990; Fukao et al., 1991; Hall et al., 1992; Hoppe and Fritts, 1995a, 1995b]. These have stimulated animated discussions and several theoretical studies based on the Stokes drift due to GWs and the potential for backscatter biases in radar measurements [Coy et al., 1986; Walterscheid and Hocking, 1991; Nastrom and VanZandt, 1994; Gibson-Wilde et al., 2000]. The latter attribute the apparent downward bias to the presence of enhanced refractive index fluctuations in the more stably stratified, and downward moving phases of the GWs accounting for the majority of atmospheric turbulence, but to date there has been no definitive explanation of these measurement biases. Other

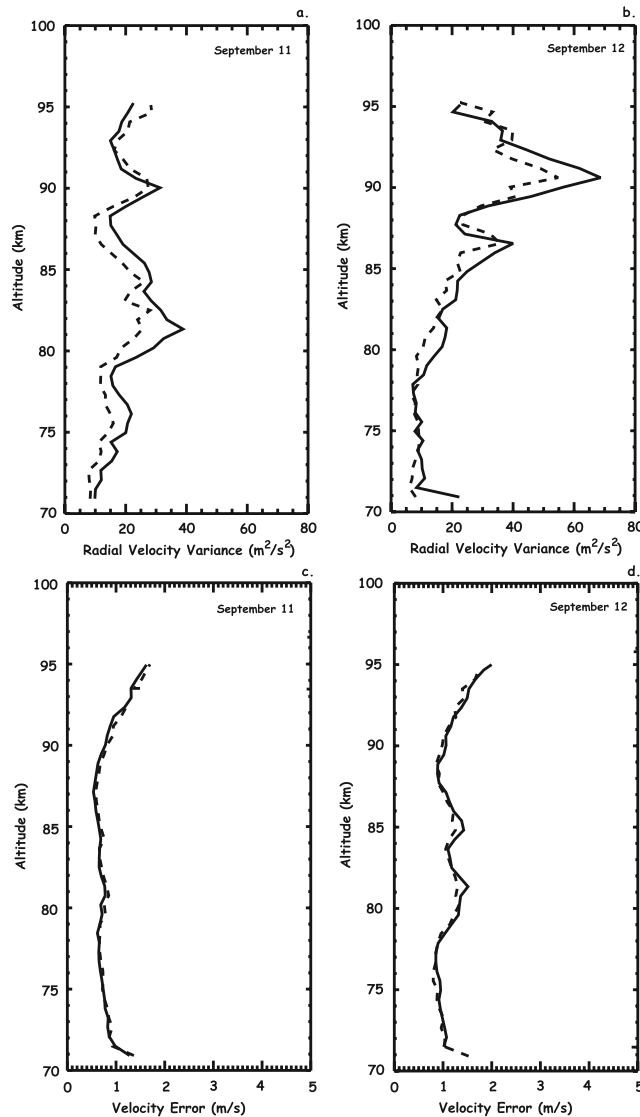


Figure 4. Radial velocity variances computed in the east (solid) and west (dashed) beams for (a) 11 and (b) 12 September after removal of the linear trends from each time series. (c and d) Radial velocity uncertainties based on the quality of the Lorentzian spectral fits for the same two days. Note that radial velocity variances are ~ 10 to 50 times the uncertainties ($S/N \sim 10$ to 50) and that error variances are essentially identical between beams, suggesting a potential for dual-beam momentum flux estimates having high confidence. The zonal momentum fluxes and their frequency dependence and temporal variability are discussed by *Fritts et al.* [2006a].

possible contributors to increasing low-frequency vertical motions at higher altitudes are the superposed tidal modes that collectively define the overall tidal response. However, these appear, on the basis of current modeling (*Hagan and Forbes* [2002, 2003] and available web-based data) to be unable to account for such large vertical motions at these altitudes. Other processes, possibly including ion layers and their motions relative to the neutral atmosphere, may also contribute, but these dynamics are largely unknown and unexplored at this time. Indeed, our present data may shed

new light on these topics, as incoherent scatter velocities should not be subject to the same measurement biases as the other radars previously used for such estimates (typically ~ 50 and 224 MHz radars) measuring either under active Polar Mesosphere Summer Echo (PMSE) conditions or in environments where stratification and GW dynamics may induce measurement biases [*Nastrom and VanZandt*, 1994; *Hoppe et al.*, 1990; *Hoppe and Fritts*, 1995a, 1995b].

[16] Vertical winds due to higher-frequency GWs cannot be inferred unambiguously, because they cannot be separated from the horizontal wind contributions by the same GWs to the radial winds in our oblique beams. There are suggestions of GW motions with amplitudes as large as ~ 3 ms^{-1} in the \sim hourly averaged vertical velocity profiles shown in Figure 6. We cannot be certain, however, that these are not a result of GWs having small vertical wavelengths (and small intrinsic phase speeds) that yield systematic horizontal wind differences in the east and west beams in the hourly profiles. The vertical scales and apparent correlations in altitude on occasion suggest that these vertical motions may be real, but there is no clear correlation with the zonal motions inferred for the same intervals. There are also indications of significant vertical motions at higher frequencies in the radial velocity data shown in Figures 2 and 3, given the different radial velocity magnitudes. As noted above, horizontal velocities contribute equal radial velocity contributions in each beam that are more typically anticorrelated between beams because of the larger horizontal scales that dominate horizontal velocity variances. Thus the differences in radial velocities noted above must reflect the contributions of vertical velocities, particularly at the higher frequencies (periods of ~ 4.5 to 20 min), and these are approximately half the difference in radial velocity amplitudes, thus a few ms^{-1} at a number of locations. In general, vertical motions may be inferred with confidence only by strictly vertical viewing or by removing the contributions to radial velocities by horizontal motions for longer averaging intervals. However, this requires suitably long averaging, because of potential horizontal variations in the structures that must be removed by assuming horizontal homogeneity, as well as the typically larger horizontal than vertical contributions to radial velocities, except at small off-zenith angles.

[17] Additional insights are provided by computing the vertical wave number spectra from the radar data. For these spectra, we employ the \sim hourly averaged horizontal wind data because lower-frequency GWs typically dominate horizontal wind variances [*Fritts and Alexander*, 2003]. Wave number spectra for each beam direction and \sim hourly profile, and the averaged spectrum for each day, are shown in Figures 7 and 8. The spectra for each vertical profile generally agree well between beams, as we expect from the consistency in the inferred zonal velocities shown in Figure 5. Each spectrum is also largely consistent with the -3 slope and the “saturated” spectral amplitude shown for reference in each panel that is characteristic of such spectra observed elsewhere as a result of GW saturation conditions [*Fritts and Alexander*, 2003]. Successive spectra are also seen to exhibit significant consistency in a number of cases, as we expect for GWs having periods of ~ 2 hours or longer. Examples include the common peaks and valleys

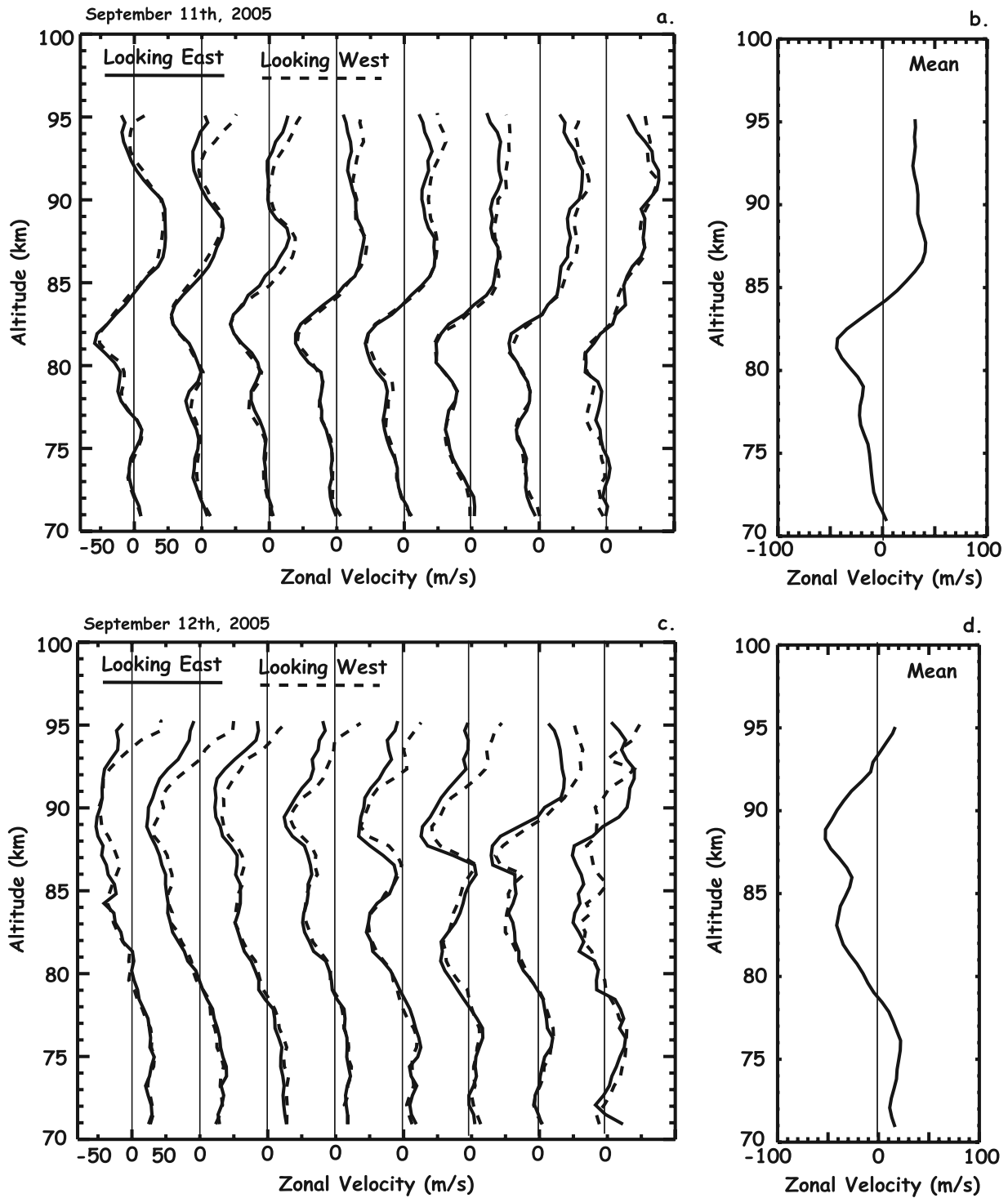


Figure 5. Zonal winds obtained from ~ 50 -min averaged radial winds in the east (solid) and west (dashed) beams and their respective daily means for (a and b) 11 and (c and d) 12 September 2005. Successive profiles are displaced by 100 ms^{-1} . Note that the Gregorian feed was directed east on 11 September and west on 12 September, so the differences above $\sim 90 \text{ km}$ are independent of the antenna. Horizontal velocity uncertainties based on spectral fitting vary from $\sim 2 \text{ ms}^{-1}$ at ~ 71 to 90 km and $\sim 4 \text{ ms}^{-1}$ above 90 km .

among spectra 2 to 4 and 5 to 8 at wavelengths of ~ 3 to 20 km on 11 September and for profiles 2 to 8 at wavelengths of ~ 5 to 20 km on 12 September. The mean spectra for each day exhibit considerably less variability and are seen to agree

reasonably with the “saturated” spectral slope of -3 noted above. There is also evidence of a possible noise floor in several of the individual spectra, and also in the mean spectra, at a spectral amplitude of $\sim 3 \times 10^{-1} \text{ m}^2 \text{ s}^{-2} \text{ km}^{-1}$ as the

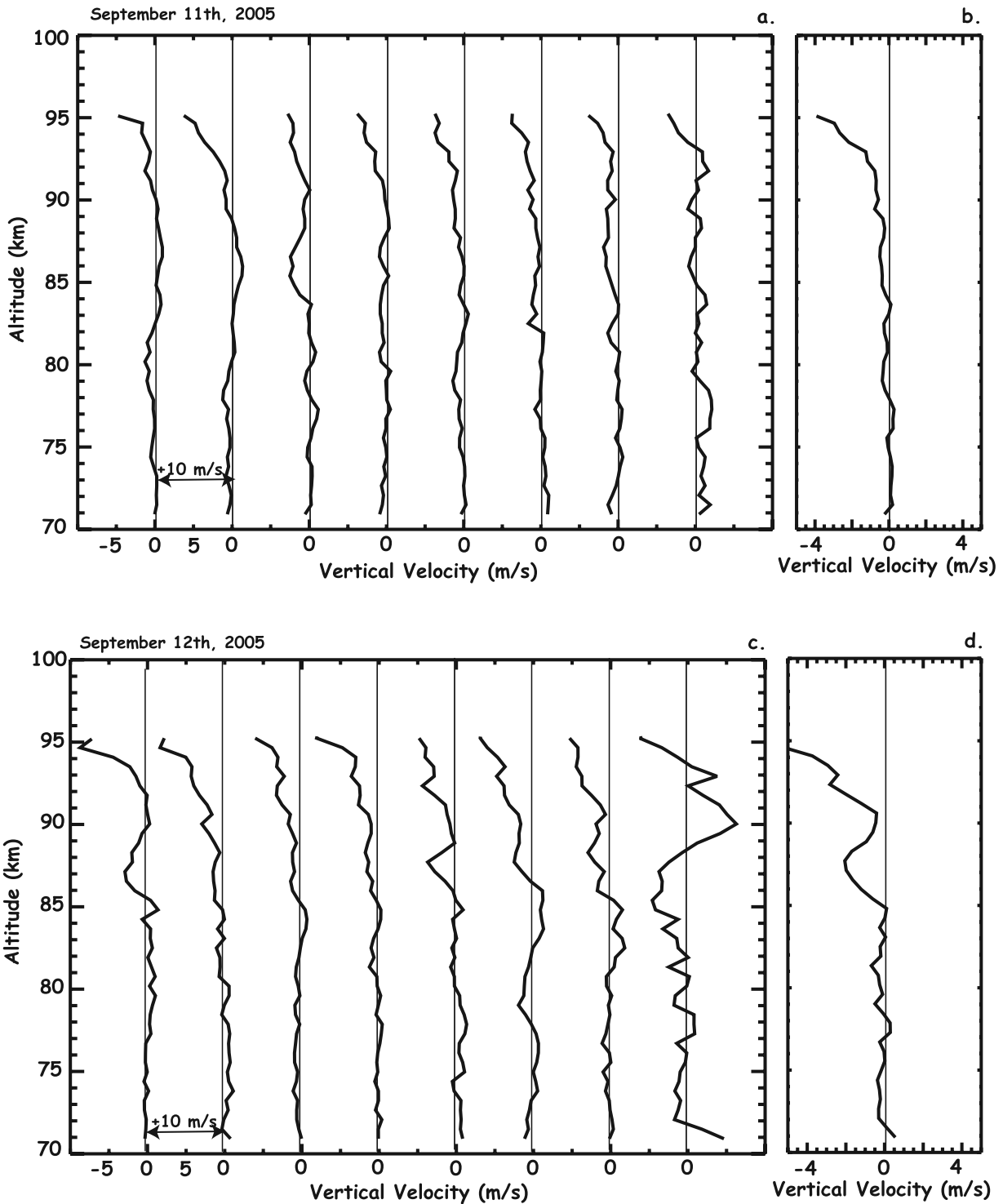


Figure 6. As in Figure 5 but for ~ 50 -min estimates of the vertical velocities employing both beams for (a and b) 11 and (c and d) 12 September. Successive profiles are displaced by 10 ms^{-1} .

Nyquist wave number is approached (especially at earlier times in Figure 7 and intermediate times in Figure 8). This appears to have a minor impact on our analysis, however.

4. Summary and Discussion

[18] The results described above represent the first comprehensive application of the new dual-beam capability for

Doppler velocity measurements in the MLT region using the AO 430 MHz ISR. The 2 MW peak transmitter power was distributed equally between the Gregorian and line feeds to establish two beams inclined 15° east and west of vertical for two ~ 7 -hour daytime measurement intervals on 11 and 12 September 2005. The beam configuration was designed specifically to allow for a measurement of momentum fluxes employing the dual-beam method pioneered by

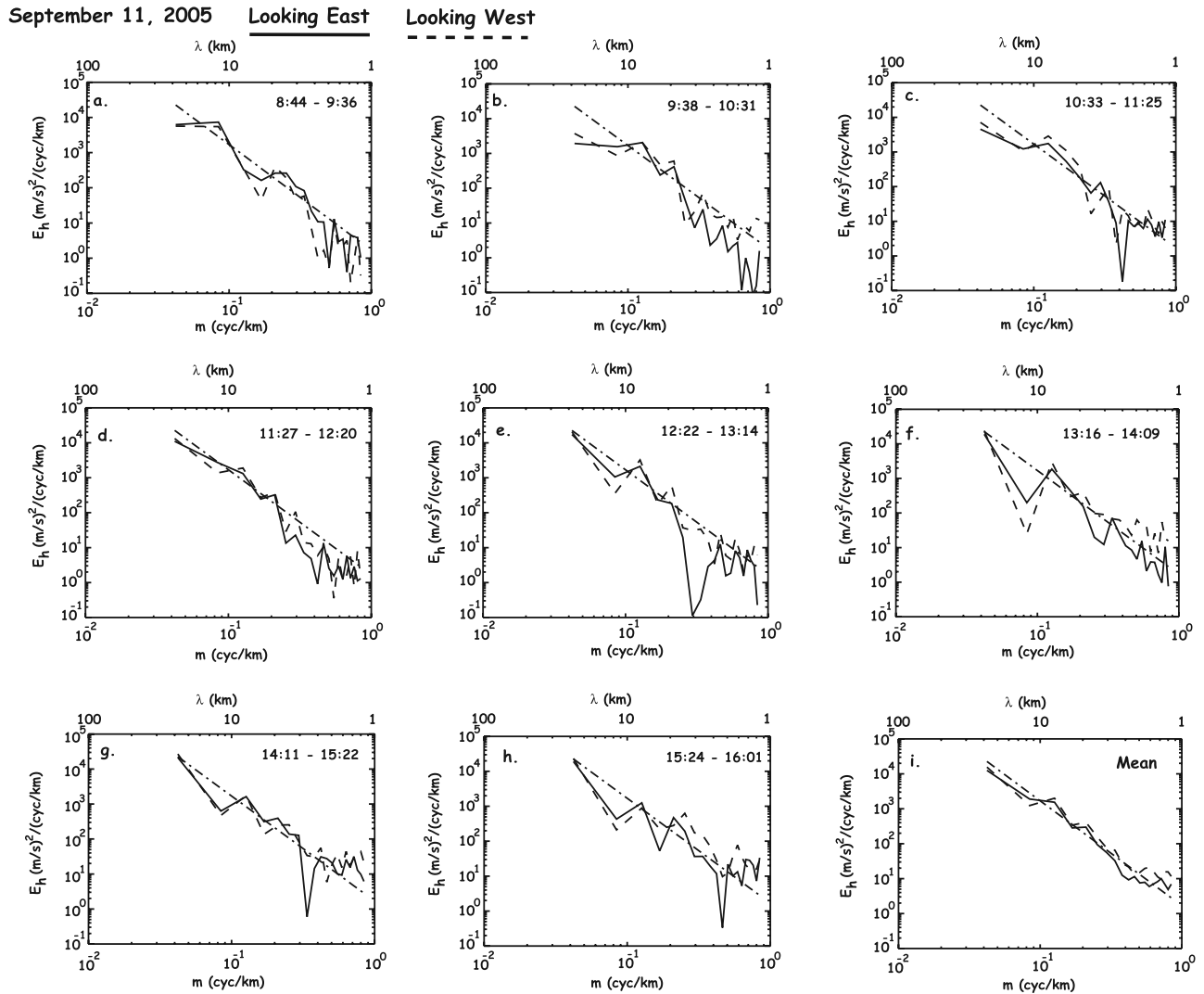


Figure 7. (a–h) Wave number spectra for 11 September 2005 computed from the ~ 50 -min averaged zonal wind profiles shown in Figure 5 and (i) the mean for all data. Solid and dashed lines are for the east and west beams, respectively, and a reference spectrum of the form $N^2/6m^3$, with $N = 2 \times 10^{-2} \text{ s}^{-1}$, expected on the basis of saturation theory (see text) is included in each panel.

Vincent and Reid [1983], and radial velocities showed no obvious disparities between beams. Indeed, the inferred zonal mean velocities agreed extremely well between the two beams when averaged over less than an hour, with differences that can be reasonably attributed to lower-frequency GWs having horizontal structures smaller than, or comparable to, the beam spacing of ~ 40 km at ~ 70 to 90-km altitudes. Fits of Lorentzian spectra to the Doppler spectra, averaged in 600-m bins, yielded radial velocity uncertainties of $\sim 1 \text{ ms}^{-1}$ over altitudes of ~ 71 to 95 km.

[19] At higher altitudes, there was an apparent downward mean vertical motion increasing from ~ 1 to 5 ms^{-1} from ~ 90 to 95 km that is consistent with similar measurements at a number of other VHF radars (cited above), though previous measurements were typically confined to altitudes near 90 km and mean vertical motions of $\sim 1 \text{ ms}^{-1}$. Various possible explanations have been explored, including (1) vertical GW Stokes drifts [Coy et al., 1986; Walterscheid and Hocking, 1991] and (2) known radar measurement

biases arising from significant correlations among backscatter power due to refractive index fluctuations, Doppler spectral widths, and the tendency for larger refractive index fluctuations to accompany the downward and more stable (and less turbulent) phase of the GWs contributing most to turbulence generation and modulation at these altitudes [Hoppe et al., 1990; Nastrom and VanZandt, 1994; Hoppe and Fritts, 1995a, 1995b]. Indeed, the likely lack of such a refractive index measurement bias in our ISR measurements may help to resolve this persistent problem in interpreting mean vertical motions measured by radars at high altitudes. This should also help establish confidence in Doppler resonance lidar measurements of mean vertical motions when measurement uncertainties allow for such estimates, as the lidars (like the ISRs) should respond to the bulk atmospheric motions rather than biased estimates dependent on radar backscatter power correlations with dynamical variables. Meteor echoes are another means of inducing an apparent downward mean motion (with sufficient Dopp-

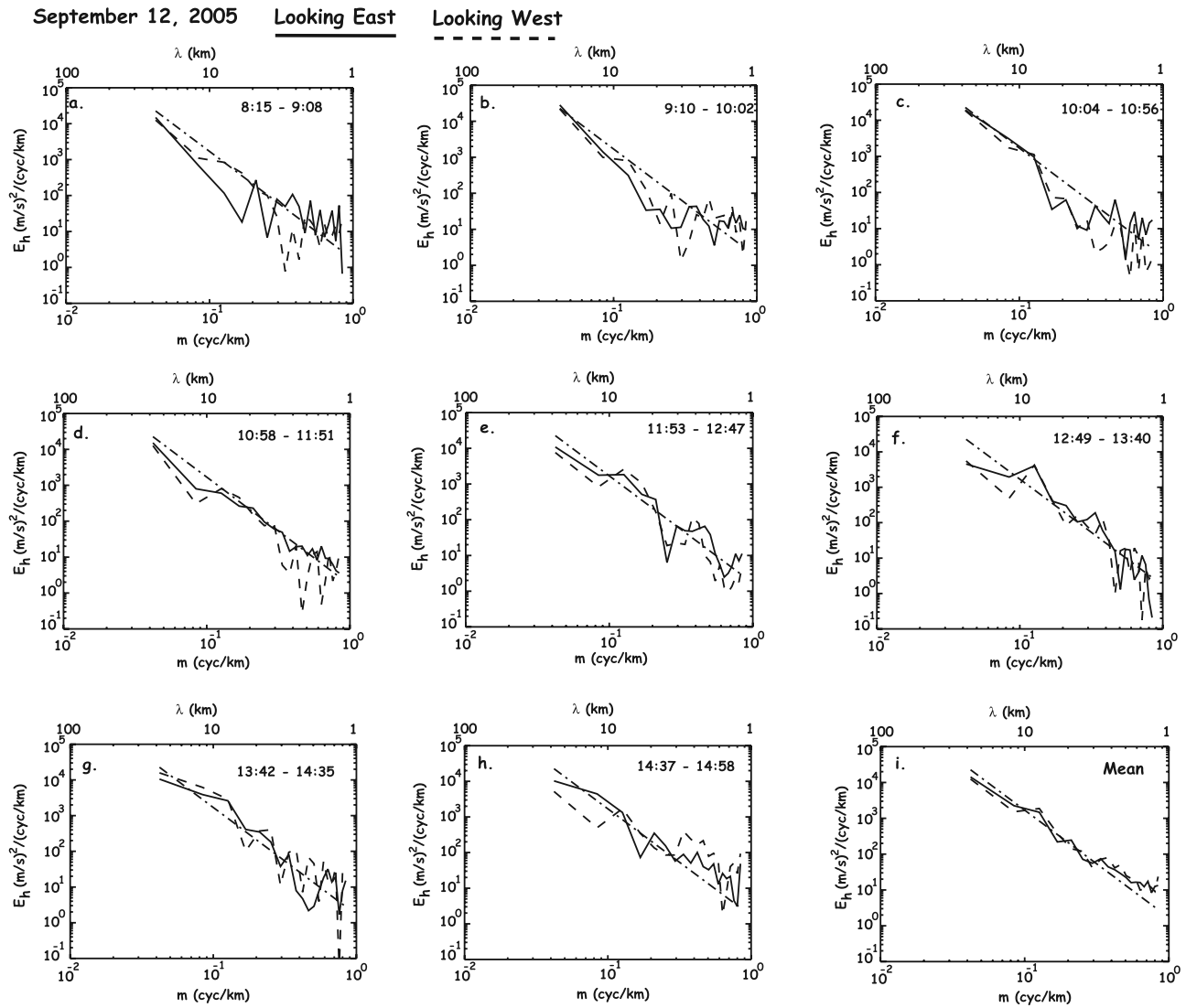


Figure 8. (a–i) As in Figure 7 but for 12 September.

ler sensitivity), but it seems unlikely to us that this contribution would have a sufficiently narrow Doppler spectrum to make a net downward contribution to our measurements. Given that mean Lagrangian motions of this magnitude are entirely impossible to reconcile with our understanding of radiative timescales and residual transports at these altitudes, we remain in need of a suitable explanation for the large apparent downward mean motions at the highest altitudes of our measurements.

[20] The GW characteristics occurring during our two observation periods had some similarities and some significant differences. In both cases, the radial velocities appeared to be dominated by the higher frequencies (typical periods of ~ 4.5 to 15 min), in large part because of their greater projections onto the small off-zenith beam angles employed for our measurements. There were also, nevertheless, significant lower-frequency GW motions that are apparent in Figures 2 and 3, but which are not emphasized as clearly because horizontal motions project only 25% of their amplitude into 15° zenith beams, while vertical motions project almost entirely into these beams. Zonal

wind estimates, which averaged over this high-frequency (largely vertical) velocity variability, exhibited relatively uniform and slowly varying structures, slower phase descents, and greater consistency between east and west beam zonal wind estimates on 11 September (Figures 5a and 5b). In contrast, zonal winds inferred on 12 September (Figures 5c and 5d) appeared to exhibit greater variability in time, greater variability between east and west beam zonal wind estimates (perhaps because of different horizontal scales), significantly higher temporal variability, and a greater tendency for large shears and inferred tendencies for instability processes. These differences were also apparent in the inferred \sim hourly mean vertical motions (Figure 6), which tended to be small on 11 September, but larger and more variable on 12 September. As noted above, we cannot be certain that these apparent differences are not simply a consequence of the different spatial variations of the GW motions on the scale of the radar beam separations at MLT altitudes. However, the greater apparent temporal variability of the zonal winds on 12 September also appears to have implications for preferred GW propagation directions, mo-

mentum fluxes, and their variability with time that is explored more fully in the companion paper by *Fritts et al.* [2006a]. The vertical wave number spectra, while often exhibiting consistency between adjacent profiles and with the slopes expected from GW saturation theory, do not obviously contribute to an understanding of the temporal variability of the GW field. They do, however, confirm the dominant contributions of the horizontal GW velocities to the total GW kinetic energy, despite the apparent dominance of the velocity fields in Figures 2 and 3 noted above.

5. Conclusions

[21] We have employed new dual-beam measurements using the AO 430 MHz radar Gregorian and line feeds for ISR Doppler velocity measurements at altitudes of ~ 71 to 95 km under daytime conditions in order to test an anticipated capability for accurate and high-resolution (in space and time) radial wind measurements that would allow for estimates of mean horizontal and vertical winds and GW perturbations and momentum fluxes at MLT altitudes. The purposes of this paper were to describe the measurement and data analysis techniques, to assess the measurement uncertainties, to demonstrate the ability to characterize the mean and lower-frequency (horizontal and vertical) mean and GW motions, to compare the character of the GW field with previous measurements and theory, and to confirm that the method enables comprehensive studies of GW dynamics and quantification of GW effects at MLT altitudes.

[22] Radial velocity uncertainties based on the accuracies of fits of Lorentzian spectra to ISR Doppler spectra confirmed that radial velocity estimates were sufficient for characterization of both the mean motions and the velocity fluctuations, as well as momentum fluxes, typically accompanying higher-frequency GW motions. The latter results are described in the companion paper by *Fritts et al.* [2006a] and suggest a potential to quantify with such measurements the correlations between GW momentum fluxes and larger-scale tidal and planetary wave motions that must provide the basis for a more comprehensive parameterization of such interactions and effects in large-scale models of the MLT and above.

[23] These results were employed in this paper to define the mean and low-frequency GW field during our two measurement intervals on 11 and 12 September 2005. Apart from differences in the GW fields and characteristics during our two measurement intervals, we believe that such ISR measurements at MLT altitudes may also be able to play an important role in assessing (and resolving) persistent, and perplexing, apparent biases in radar measurements of mean vertical velocities that cannot be reconciled with strong radiative constraints at the same altitudes. Essentially, the inferred mean downward motions increasing from ~ 1 to 5 ms^{-1} between ~ 90 and 95-km altitudes imply adiabatic heating rates of ~ 1000 to 5000 K day^{-1} , and are clearly incompatible with any real mean vertical motion and corresponding adiabatic response. To date, however, observations have not provided sufficient guidance for theoretical efforts, and these new measurements, together with others by radars exhibiting known biases, and lidars that we believe to be free of such measurement biases, may contribute to the resolution of this dilemma, among others.

[24] **Acknowledgments.** Support for this research by D.J. was provided under agreement 34560-7826 between Cornell University and North-West Research Associates, and the prime sponsor is NSF under agreement AST-9809484. The Arecibo Observatory is part of the National Astronomy and Ionosphere Center, which is operated by Cornell University under cooperative agreement with the National Science Foundation. Support for DCF was provided under NSF grant ATM-0436703, NASA contract NASS-02036, and AFOSR contract F49620-03-C-0045. Support for D.M.R. was provided under NASA contract NNH05CC70C.

References

- Andreassen, O., C.-E. Wasberg, D. C. Fritts, and J. R. Isler (1994), Gravity wave breaking in two and three dimensions: 1. Model description and comparison of two-dimensional evolutions, *J. Geophys. Res.*, *99*, 8095–8108.
- Andreassen, O., P. O. Hvidsten, D. C. Fritts, and S. Arendt (1998), Vorticity dynamics in a breaking gravity wave, 1. Initial instability evolution, *J. Fluid Mech.*, *367*, 27–46.
- Balsley, B. B., and A. C. Riddle (1984), Monthly mean values of the mesospheric wind field over Poker Flat, Alaska, *J. Atmos. Sci.*, *41*, 2368–2375.
- Coy, L., D. C. Fritts, and J. Weinstock (1986), The Stokes drift due to vertically propagating internal gravity waves in a compressible atmosphere, *J. Atmos. Sci.*, *43*, 2636–2643.
- Djuth, F. T., M. P. Sulzer, J. H. Elder, and V. P. Wickwar (1997), High-resolution studies of atmosphere-ionosphere coupling at Arecibo Observatory, Puerto Rico, *Radio Sci.*, *32*, 2321–2344.
- Djuth, F. T., M. P. Sulzer, S. A. Gonzales, J. D. Mathews, J. H. Elder, and R. L. Walterscheid (2004), A continuum of gravity waves in the Arecibo thermosphere?, *Geophys. Res. Lett.*, *31*, L16801, doi:10.1029/2003GL019376.
- Forbes, J. M., J. Gu, and S. Miyahara (1991), On the interactions between gravity waves and the diurnal propagating tide, *Planet. Space Sci.*, *39*, 1249–1257.
- Fritts, D. C., and M. J. Alexander (2003), Gravity wave dynamics and effects in the middle atmosphere, *Rev. Geophys.*, *41*(1), 1003, doi:10.1029/2001RG000106.
- Fritts, D. C., and G. D. Nastrom (1992), Sources of mesoscale variability of gravity waves, II: Frontal, convective, and jet stream excitation, *J. Atmos. Sci.*, *49*, 111–127.
- Fritts, D. C., and R. A. Vincent (1987), Mesospheric momentum flux studies at Adelaide, Australia: Observations and a gravity wave/tidal interaction model, *J. Atmos. Sci.*, *44*, 605–619.
- Fritts, D. C., and L. Yuan (1989), Measurement of momentum fluxes near the summer mesopause at Poker Flat, Alaska, *J. Atmos. Sci.*, *46*, 2569–2579.
- Fritts, D. C., U.-P. Hoppe, and B. Inhester (1990), A study of the vertical motion field near the high-latitude summer mesopause during MAC/SINE, *J. Atmos. Terr. Phys.*, *52*, 927–938.
- Fritts, D. C., J. R. Isler, G. E. Thomas, and O. Andreassen (1993), Wave breaking signatures in noctilucent clouds, *Geophys. Res. Lett.*, *20*, 2039–2042.
- Fritts, D. C., J. R. Isler, and O. Andreassen (1994), Gravity wave breaking in two and three dimensions: 2. Three-dimensional evolution and instability structure, *J. Geophys. Res.*, *99*, 8109–8123.
- Fritts, D. C., J. F. Garten, and O. Andreassen (1996), Wave breaking and transition to turbulence in stratified shear flows, *J. Atmos. Sci.*, *53*, 1057–1085.
- Fritts, D. C., S. Arendt, and O. Andreassen (1998), Vorticity dynamics in a breaking internal gravity wave, 2. Vortex interactions and transition to turbulence, *J. Fluid Mech.*, *367*, 47–65.
- Fritts, D. C., S. L. Vadas, and Y. Yamada (2002), An estimate of strong local body forcing and gravity wave radiation based on OH airglow and meteor radar observations, *Geophys. Res. Lett.*, *29*(10), 1429, doi:10.1029/2001GL013753.
- Fritts, D. C., C. Bizon, J. A. Werne, and C. K. Meyer (2003), Layering accompanying turbulence generation due to shear instability and gravity wave breaking, *J. Geophys. Res.*, *108*(D8), 8452, doi:10.1029/2002JD002406.
- Fritts, D. C., D. Janches, D. M. Riggin, M. P. Sulzer, and S. Gonzales (2006a), Gravity waves and momentum fluxes in the mesosphere and lower thermosphere using 430 MHz dual-beam measurements at Arecibo: 2. Frequency spectra, momentum fluxes, and variability, *J. Geophys. Res.*, *111*, D18108, doi:10.1029/2005JD006883.
- Fritts, D. C., S. L. Vadas, K. Wan, and J. A. Werne (2006b), Mean and variable forcing of the middle atmosphere by gravity waves, *J. Atmos. Sol. Terr. Phys.*, *68*, 247–265.
- Fukao, S., Y. Maekawa, T. Sato, and S. Kato (1985), Fine structure in mesospheric wind fluctuations observed by the Arecibo UHF Doppler radar, *J. Geophys. Res.*, *90*, 7547–7556.

- Fukao, S., M. F. Larsen, M. D. Yamanaka, H. Furukawa, T. Tsuda, and S. Kato (1991), Observations of a reversal in long-term average vertical velocities near the jetstream wind maximum, *Mon. Weather Rev.*, *119*, 1479–1489.
- Fukuyama, K. (1981), Incoherent scatter radar observations of wavelike structures in the mesosphere over Arecibo, *J. Geophys. Res.*, *86*, 9152–9158.
- Ganguly, S. (1980), Incoherent scatter radar observations of mesospheric dynamics at Arecibo, *Geophys. Res. Lett.*, *7*, 369–372.
- Garcia, R. R., and S. Solomon (1985), The effect of breaking gravity waves on the dynamics and chemical composition of the mesosphere and lower thermosphere, *J. Geophys. Res.*, *90*, 3850–3868.
- Gibson-Wilde, D. E., J. A. Werne, D. C. Fritts, and R. J. Hill (2000), Direct numerical simulation of VHF radar measurements of turbulence in the mesosphere, *Radio Sci.*, *35*, 783–798.
- Green, J. L., K. S. Gage, T. E. VanZandt, W. L. Clark, J. M. Warnock, and G. D. Nastrom (1988), Observations of vertical velocity over Illinois by the Flatland radar, *Geophys. Res. Lett.*, *15*, 269–272.
- Hagan, M. E., and J. M. Forbes (2002), Migrating and nonmigrating diurnal tides in the middle and upper atmosphere excited by tropospheric latent heat release, *J. Geophys. Res.*, *107*(D24), 4754, doi:10.1029/2001JD001236.
- Hagan, M. E., and J. M. Forbes (2003), Migrating and nonmigrating semi-diurnal tides in the upper atmosphere excited by tropospheric latent heat release, *J. Geophys. Res.*, *108*(A2), 1062, doi:10.1029/2002JA009466.
- Hall, T. M., J. Y. N. Cho, M. C. Kelley, and E. K. Hocking (1992), A reevaluation of the Stokes drift in the polar summer mesosphere, *J. Geophys. Res.*, *97*(D1), 887–897.
- Hecht, J. H. (2004), Instability layers and airglow imaging, *Rev. Geophys.*, *42*, RG1001, doi:10.1029/2003RG000131.
- Hecht, J. H., R. L. Walterscheid, D. C. Fritts, J. R. Isler, D. C. Senft, C. S. Gardner, and S. J. Franke (1997), Wave breaking signatures in OH airglow and sodium densities and temperatures: 1. Airglow imaging, Na lidar, and MF radar observations, *J. Geophys. Res.*, *102*, 6655–6668.
- Hecht, J. H., C. Fricke-Bergemann, and R. L. Walterscheid (2000), Observations of the breakdown of an atmospheric gravity wave near the cold summer mesopause at 54°N, *Geophys. Res. Lett.*, *27*, 879–882.
- Hecht, J. H., A. Z. Liu, R. L. Walterscheid, and R. J. Rudy (2005), Maui Mesosphere and Lower Thermosphere (Maui MALT) observations of the evolution of Kelvin-Helmholtz billows formed near 86 km altitude, *J. Geophys. Res.*, *110*, D09S10, doi:10.1029/2003JD003908.
- Hitchman, M. H., J. C. Gille, C. D. Rodgers, and G. Brasseur (1989), The separated polar winter stratopause: A gravity wave driven climatological feature, *J. Atmos. Sci.*, *46*, 410–422.
- Hocke, K., and K. Schlegel (1996), A review of atmospheric gravity waves and traveling ionospheric disturbances: 1982–1995, *Ann. Geophys.*, *14*, 917–940.
- Holton, J. R. (1982), The role of gravity wave induced drag and diffusion in the momentum budget of the mesosphere, *J. Atmos. Sci.*, *39*, 791–799.
- Hoppe, U.-P., and D. C. Fritts (1995a), On the downward bias in vertical velocity measurements by VHF radars, *Geophys. Res. Lett.*, *22*, 619–622.
- Hoppe, U.-P., and D. C. Fritts (1995b), High-resolution measurements of vertical velocity with the EISCAT VHF radar: 1. Motion field characteristics and measurement biases, *J. Geophys. Res.*, *100*, 16,813–16,826.
- Hoppe, U.-P., D. C. Fritts, I. M. Reid, P. Czechowsky, C. M. Hall, and T. L. Hansen (1990), Multiple-frequency studies of the high-latitude summer mesosphere: Implications for scattering processes, *J. Atmos. Terr. Phys.*, *52*, 907–926.
- Kim, Y.-J., S. D. Eckermann, and H.-Y. Chun (2003), An overview of the past, present and future of gravity-wave drag parameterization for numerical climate and weather prediction models, *Atmos. Ocean*, *41*, 65–98.
- Klostermeyer, J. (1991), Two- and three-dimensional parametric instabilities in finite amplitude internal gravity waves, *Geophys. Astrophys. Fluid Dyn.*, *64*, 1–25.
- Larsen, M. F. (2000), Coqui 2: Mesospheric and lower thermospheric wind observations over Puerto Rico, *Geophys. Res. Lett.*, *27*, 445–448.
- Li, F., A. Z. Liu, and G. R. Swenson (2005a), Characteristics of instabilities in the mesopause region over Maui, Hawaii, *J. Geophys. Res.*, *110*, D09S12, doi:10.1029/2004JD005097.
- Li, F., A. Z. Liu, G. R. Swenson, J. H. Hecht, and W. A. Robinson (2005b), Observations of gravity wave breakdown into ripples associated with dynamical instabilities, *J. Geophys. Res.*, *110*, D09S11, doi:10.1029/2004JD004849.
- Li, T., C. Y. She, B. P. Williams, T. Yuan, R. L. Collins, L. M. Kieffaber, and A. W. Peterson (2005c), Concurrent OH imager and sodium temperature/wind lidar observation of localized ripples over northern Colorado, *J. Geophys. Res.*, *110*, D13110, doi:10.1029/2004JD004885.
- Lombard, P. N., and J. J. Riley (1996), Instability and breakdown of internal gravity waves. I. Linear stability analysis, *Phys. Fluids*, *8*, 3271–3287.
- Lu, W., and D. C. Fritts (1993), Spectral estimates of gravity wave energy and momentum fluxes, III: Gravity wave-tidal interactions, *J. Atmos. Sci.*, *50*, 3714–3727.
- Mathews, J. D. (1976), Measurements of the diurnal tides in the 80 to 100-km altitude range at Arecibo, *J. Geophys. Res.*, *81*, 4671–4677.
- Mathews, J. D., M. P. Sulzer, and P. Perillat (1997), Aspects of layer electrodynamic inferred from high-resolution ISR observations of the 80–270 km ionosphere, *Geophys. Res. Lett.*, *24*, 1411–1414.
- Mayr, H. G., J. G. Mengel, K. L. Chan, and H. S. Porter (1998), Seasonal variations of the diurnal tide induced by gravity wave filtering, *Geophys. Res. Lett.*, *25*, 943–946.
- McIntyre, M. E. (1989), On dynamics and transport near the polar mesopause in summer, *J. Geophys. Res.*, *94*, 14,617–14,628.
- McLandress, C. (2002), The seasonal variation of the propagating diurnal tide in the mesosphere and lower thermosphere. Part I: The role of gravity waves and planetary waves, *J. Atmos. Sci.*, *59*, 893–906.
- McLandress, C., and W. E. Ward (1994), Tidal/gravity wave interactions and their influence on the large-scale dynamics of the middle atmosphere: Model results, *J. Geophys. Res.*, *99*, 8139–8156.
- Meek, C. E., and A. H. Manson (1989), Rhythmic motions in the upper middle atmosphere from the Saskatoon (52°N, 107°W) M.F. radar, *J. Atmos. Sci.*, *46*, 849–858.
- Meyer, C. K. (1999a), Gravity wave interactions with the diurnal propagating tide, *J. Geophys. Res.*, *104*, 4223–4239.
- Meyer, C. K. (1999b), Gravity wave interactions with mesospheric planetary waves: A mechanism for penetration into the thermosphere-ionosphere system, *J. Geophys. Res.*, *104*, 28,181–28,196.
- Murphy, D. J., and R. A. Vincent (1998), Mesospheric momentum fluxes over Adelaide during the 2-day wave: Results and interpretation, *J. Geophys. Res.*, *103*, 28,627–28,636.
- Nakamura, T., D. C. Fritts, J. R. Isler, T. Tsuda, and R. A. Vincent (1997), Short-period fluctuations of the diurnal tide observed with low-latitude MF and meteor radars during CADRE: Evidence for gravity wave/tidal interactions, *J. Geophys. Res.*, *102*, 26,225–26,238.
- Nastrom, G. D., and T. E. VanZandt (1994), Mean vertical motions seen by radar wind profiles, *J. Appl. Meteorol.*, *33*, 984–995.
- Nastrom, G. D., W. L. Ecklund, and K. S. Gage (1985), Direct measurement of large-scale vertical velocities using clear-air Doppler radars, *Mon. Weather Rev.*, *113*, 708–718.
- Nicolls, M. J., and M. C. Kelley (2005), Strong evidence for gravity wave seeding of an ionospheric plasma instability, *Geophys. Res. Lett.*, *32*, L05108, doi:10.1029/2004GL020737.
- Oliver, W. L., Y. Otsuka, M. Sato, T. Takami, and S. Fukao (1997), A climatology of F region gravity wave propagation over the Middle and Upper Atmosphere Radar, *J. Geophys. Res.*, *102*, 14,499–14,512.
- Rüster, R., and I. M. Reid (1990), VHF radar observations of the dynamics of the summer polar mesopause region, *J. Geophys. Res.*, *95*, 10,005–10,016.
- Sonmor, L. J., and G. P. Klaassen (1997), Toward a unified theory of gravity wave stability, *J. Atmos. Sci.*, *54*, 2655–2680.
- Swenson, G. R., and S. B. Mende (1994), OH emission and gravity waves (including a breaking wave) in all-sky imagery from Bear Lake, UT, *Geophys. Res. Lett.*, *21*, 2239–2242.
- Vadas, S. L., and D. C. Fritts (2001), Gravity wave radiation and mean responses to local body forces in the atmosphere, *J. Atmos. Sci.*, *58*, 2249–2279.
- Vadas, S. L., and D. C. Fritts (2002), The importance of spatial variability in the generation of secondary gravity waves from local body forces, *Geophys. Res. Lett.*, *29*(20), 1984, doi:10.1029/2002GL015574.
- Vadas, S. L., D. C. Fritts, and M. J. Alexander (2003), Mechanism for the generation of secondary waves in wave breaking regions, *J. Atmos. Sci.*, *60*, 194–214.
- Vincent, R. A., and I. M. Reid (1983), HF Doppler measurements of mesospheric momentum fluxes, *J. Atmos. Sci.*, *40*, 1321–1333.
- Walterscheid, R. L. (1981), Inertio-gravity wave induced accelerations of mean flow having an imposed periodic component: Implications for tidal observations in the meteor region, *J. Geophys. Res.*, *86*, 9698–9706.
- Walterscheid, R. L., and W. K. Hocking (1991), Stokes diffusion by atmospheric internal gravity waves, *J. Atmos. Sci.*, *48*, 2213–2230.
- Wang, D.-Y., and D. C. Fritts (1990), Mesospheric momentum fluxes observed by the MST radar at Poker Flat, Alaska, *J. Atmos. Sci.*, *47*, 1511–1521.
- Wang, D.-Y., and D. C. Fritts (1991), Evidence of gravity wave–tidal interaction observed near the summer mesopause at Poker Flat, Alaska, *J. Atmos. Sci.*, *48*, 572–583.
- Williams, B. P., M. A. White, D. A. Krueger, and C. Y. She (2002), Observation of a large amplitude wave and inversion layer leading to convective instability in the mesopause region over Fort Collins, CO (41°N, 105°W), *Geophys. Res. Lett.*, *29*(17), 1850, doi:10.1029/2001GL014514.

- Woodman, R. F., and A. Guillen (1974), Radar observations of winds and turbulence in the stratosphere and mesosphere, *J. Atmos. Sci.*, *31*, 493–505.
- Yamada, Y., H. Fukunishi, T. Nakamura, and T. Tsuda (2001), Breakdown of small-scale quasi-stationary gravity wave and transition to turbulence observed in OH airglow, *Geophys. Res. Lett.*, *28*, 2153–2156.
- Zhou, Q. H. (2000), Incoherent scatter radar measurement of vertical winds in the mesosphere, *Geophys. Res. Lett.*, *27*, 1803–1806.
- Zhou, Q. H., M. P. Sulzer, and C. A. Tepley (1997), An analysis of tidal and planetary waves in the neutral winds and temperature observed at low-latitude E region heights, *J. Geophys. Res.*, *102*(A6), 11,491–11,506.
-
- D. C. Fritts, D. Janches, and D. M. Riggin, Colorado Research Associates, NorthWest Research Associates, 3380 Mitchell Lane, Boulder, CO 80301, USA. (diego@cora.nwra.com)
- S. Gonzalez and M. P. Sulzer, Arecibo Observatory, National Astronomy and Ionosphere Center, HC3 Box 53995, Arecibo, Puerto Rico 00612.